Dosimetry Estimations for ^{123}I-IAZA in Healthy Volunteers

Daria Stypinski, Steve A. McQuarrie, Leonard I. Wiebe, Yun K. Tam, John R. Mercer, and Alexander J.B. McEwan

MDS Pharma Services, Lincoln, Nebraska; Faculty of Pharmacy and Pharmaceutical Sciences and Faculty of Medicine, University of Alberta, Edmonton, Alberta; and Cross Cancer Institute, Edmonton, Alberta, Canada

^{123}I-Labeled iodoazomycin arabinoside (IAZA) is a marker of hypoxia in vivo. It has been used clinically to image hypoxic tissue in solid tumors, peripheral vascular disease of diabetic origin, blunt brain trauma, and rheumatoid joints and in an animal model of cerebrovascular disease. The radiation dose biodistribution for ^{123}I-IAZA was studied to assess and characterize its suitability as a clinical radiopharmaceutical. **Methods:** Six healthy volunteers each received a nominal 185-MBq (5 mCi) dose of ^{123}I-IAZA administered as a slow (1–3 min) intravenous injection in the arm. Anterior and posterior whole-body planar images were acquired for each volunteer beginning immediately after injection and at 1–2, 3–4, 6–8, and 20–24 h after injection. Venous blood samples (0 h predose through 28 h after dosing) and 28-h cumulative urine samples were taken from each volunteer for pharmacokinetic analysis. Radiation dose estimates were performed for all volunteers, with "reference adult" (for men) and "adult female" (for women) phantoms, and both the International Commission on Radiological Protection 30 gastrointestinal tract model and the dynamic bladder model, using the MIRDOSE3 program. Two sets of estimates, 1 using a pharmacokinetic analysis of total serum radioactivity and 1 based on scintigraphic image data, were obtained for each volunteer after ^{123}I-IAZA administration. **Results:** Two compartments were discernible by pharmacokinetic analysis, and 4 compartments were discernible by image analysis. The urinary bladder wall received the greatest radiation dose (6.3E-02 ± 8.7E-03 mGy/MBq), followed by the upper large intestinal wall (5.6E-02 ± 1.2E-02 mGy/MBq), the lower large intestinal wall (5.0E-02 ± 1.2E-02 mGy/MBq), and the thyroid (4.4E-02 ± 1.4E-02 mGy/MBq). Approximately 90% of physiologically eliminated radioactivity was excreted through the kidneys. Radioactivity entering the intestinal tract from the gallbladder constituted <10% of biologically eliminated activity. **Conclusion:** The dosimetric analysis of ^{123}I-IAZA in 6 healthy volunteers indicated that both disposition kinetics and radiation dosimetry support its clinical use for imaging tissue hypoxia.

Key Words: radiation dosimetry; hypoxia; pharmacokinetics; radiopharmaceuticals; ^{123}I-iodoazomycin arabinoside

J Nucl Med 2001; 42:1418–1423

Although originally developed for imaging regional hypoxia in patients with cancer (*1–5*), ^{123}I-iodoazomycin arabinoside (IAZA) has also been used clinically to image hypoxic tissue in peripheral vascular disease of diabetic origin (*6*), blunt brain trauma (*7*), and rheumatoid joints (*8*) and in an animal model of cerebrovascular disease (*9,10*).

Radiation dosimetry calculations used to predict the radiation dose for patients receiving the radiopharmaceutical take into account radiation type and half-life, the amount of radioactivity administered, and tracer kinetics, including source organ identification and their respective biologic half-lives. Target organ mass, shape, and location and the intraorgan absorbed fraction of energy emitted by all source organs are usually estimated from scintigraphic images. Organ-specific parameters (S values) for a variety of human phantoms and radioisotopes have been published (*11*) and are conveniently available in the MIRDOSE computer program (Oak Ridge Institute of Science and Education, Oak Ridge, TN). Stypinski et al. (*12*) reported the clinical pharmacokinetics of IAZA, the radiopharmacokinetics of ^{123}I-IAZA, and total radioactivity kinetics for 6 healthy volunteers. The ^{123}I-IAZA radiation dosimetry estimates for those 6 volunteers are reported in this article, and this dosimetric information is compared with the previously reported pharmacokinetic data.

MATERIALS AND METHODS

Chemicals and Reagents

IAZA was synthesized and radiolabeled using published procedures established in our laboratory (*1,13*).

Clinical and Imaging Protocols

The research was conducted in accordance with the tenets of the Declaration of Helsinki (1964) and was approved by the Alberta Cancer Board Research Ethics Committee and the University of Alberta Radiation Safety Committee. Details of the clinical protocol have been described elsewhere (*12*). Six healthy volunteers (4 men, 2 women; age range, 26–54 y; mean age, 37 ± 13 y) participated with informed consent. Lugol's solution (0.6 mL, U.S. Pharmacopeia) in orange juice was given orally to block uptake of radioiodide by the thyroid, and shortly thereafter, each subject received a nominal 185-MBq (5 mCi) dose of ^{123}I-IAZA administered as a slow (1–3 min) intravenous injection in the arm.

Anterior and posterior whole-body planar images were acquired at 5 different time periods beginning immediately after injection and at 1–2, 3–4, 6–8, and 20–24 h after injection. All image times were 30 min. The images were acquired using a dual-head, large-field-of-view gamma camera (Odyssey 2000; Picker International Canada, Inc., Brampton, Ontario, Canada) equipped with a low-energy, all-purpose collimator and interfaced to an Odyssey com-

Received Nov. 14, 2000; revision accepted May 2, 2001.

For correspondence or reprints contact: Steve A. McQuarrie, PhD, 3118 Dentistry/Pharmacy Center, University of Alberta, Edmonton, Alberta, Canada T6G 2N8.

puter (Picker International Canada). The 20% analysis window was set symmetrically over the 159-keV ^{123}I photopeak.

Fourteen venous blood samples, from 0 h (predose) through 28 h after dosing, and 28-h cumulative urine samples were taken for pharmacokinetic analysis from each volunteer (*12*).

Planar scintigraphic images were exported to a personal computer equipped with MEDisplay (version 1.32s; C-Soft, Edmonton, Alberta, Canada), a medical image analysis package. The number of counts and pixels in selected regions of interest (ROIs) were obtained for each volunteer: liver, left kidney, large intestine, urinary bladder, thyroid, gallbladder, and the whole body (WB). WB counts were determined by drawing a contour around the entire body image. An off-body region drawn to the right of the volunteer's head was used as instrumental background. To partially compensate for source organ overlap, several overlapping ROIs were included: a region of overlap between the right kidney and liver, a region of left kidney with large intestine overlap, and a region of left kidney where there was no large intestine overlap. The right kidney and liver overlap ROI was established by drawing 2 parallel lines through the patient's body: 1 line passing through the uppermost point of the left kidney and the other passing through the lowest point of the liver. The left kidney region between the 2 lines was drawn, flipped around its horizontal axis, and dragged to the anatomic position of the right kidney, between the 2 lines. The count contribution from the blood pool to the organ activity was included as part of the organ activity for all ROIs.

Dosimetry Protocols

Because SPECT or CT images were not available for the volunteers, assigning activity to organs with overlapping regions as viewed from a planar 2-dimensional image was based on assumptions that were dependent on image time. The analyses initially were performed manually, and once the protocol was established all calculations were reanalyzed using Excel (version 7.0; Microsoft, Redmond, WA) for Windows 95 (Microsoft). The detailed protocol used to estimate source region activity and overlapping activity distributions is available.

Once the posterior and anterior counts in each organ were determined, the counts were further corrected by subtracting instrumental background activity (as counts per pixel) from the counts-per-pixel organ activity. The geometric mean counts for each organ were then calculated. No linear attenuation correction was made for the anterior and posterior tissues (i.e., bone, muscle, fat, and skin) above or below the organ of interest.

To determine the fractions of radioactivity entering the gut and the bladder, the dosimetry equations include WB, total body (TB), and all body (AB). TB and AB counts were determined from the anterior and posterior images at each acquisition time:

$$\text{TB counts} = \text{WB counts} - (\text{gastrointestinal tract counts} + \text{bladder counts}). \quad \text{Eq. 1}$$

Gastrointestinal tract counts consisted of the sum of the geometric mean of counts in the large intestine and the gallbladder. AB counts were determined according to the formula:

$$\text{AB counts} = \text{WB counts} - \text{bladder counts}. \quad \text{Eq. 2}$$

It is important to state at the outset that the pharmacokinetic mean residence time (MRT) and the radiation dosimetry residence time (RT) have somewhat different meanings (*14*). The RT is the area under a source organ's time–activity curve divided by the administered activity, whereas the pharmacokinetic MRT may be defined as the area under the concentration–time moment curve divided by the area under the concentration–time curve.

Once the geometric mean counts in an organ were determined for all 5 imaging times, the MRT of the radioactivity in the organ was determined using LAGRAN (version 1.0D; C. Ediss, University of Alberta, Edmonton, Alberta, Canada) (*15*), by area under the curve (AUC) integration of the ROI count versus time plot. The RT was calculated for the large intestine, liver, kidney, thyroid, WB, AB, and TB. Because each image acquisition took 30 min, it was assumed that the mean count in an organ corresponded to the midtime of 15 min after the start of image acquisition. The only exception was the thyroid, for which it was assumed that the mean counts were acquired at 5 min from the image start.

The 3 regions of interest, WB, TB, and AB, all include the counts from the liver, kidneys, and thyroid. To account for the activity in the body that is not in these organs and has not been excreted into the bladder or the gastrointestinal tract, the remainder of the body (RB) was included as an additional source organ. The RT_{fr} of this source organ was calculated as:

$$RT_{fr(RB)} = RT_{(TB)} - [RT_{fr(liver)} + RT_{fr(kidneys)} + RT_{fr(thyroid)}]. \quad \text{Eq. 3}$$

Renal and Gastrointestinal Tract Excretion Fractions

The fraction of the radioactive dose eliminated through the hepatobiliary system into the intestinal tract was determined from the gamma camera images by first calculating the rate of elimination of radioactivity into the gut (K_{gut}), according to the formula:

$$K_{gut} = \frac{1}{RT_{(AB)}} - \frac{1}{RT_{(TB)}}. \quad \text{Eq. 4}$$

Thus, the fraction of radioactive dose eliminated by the gut was determined as:

$$\text{fraction into gut} = K_{gut} \times RT_{(TB)}. \quad \text{Eq. 5}$$

Because the only other biologic route of excretion from the body available for a radiopharmaceutical is the kidneys, the fraction entering the bladder was calculated as:

$$\text{fraction into bladder} = 1 - \text{fraction into gut}. \quad \text{Eq. 6}$$

Radiation dose estimates were performed for all volunteers using the MIRDOSE3.1 program. The phantoms used were "reference adult" for the male volunteers and "adult female" for the female volunteers. The model used for analysis included a combination of both the International Commission on Radiological Protection 30 gastrointestinal tract model and the dynamic bladder model (*16*). Two sets of estimates were performed for each volunteer, one using a 2-h and one using a 4.8-h bladder void time.

RESULTS

Immediate and 22-h anterior and posterior gamma camera images of volunteer 3 are shown in Figure 1. Typically, on the earliest images, the organs with the highest radioactivity accumulation were the bladder, liver, and kidneys. The heart was visible in early images, but not at longer times; therefore, the heart activity was attributed to blood pool. The intravenous injection site also was visible on the immediate images of this volunteer, but the percentage of radioactive dose in that area, as determined by image anal-

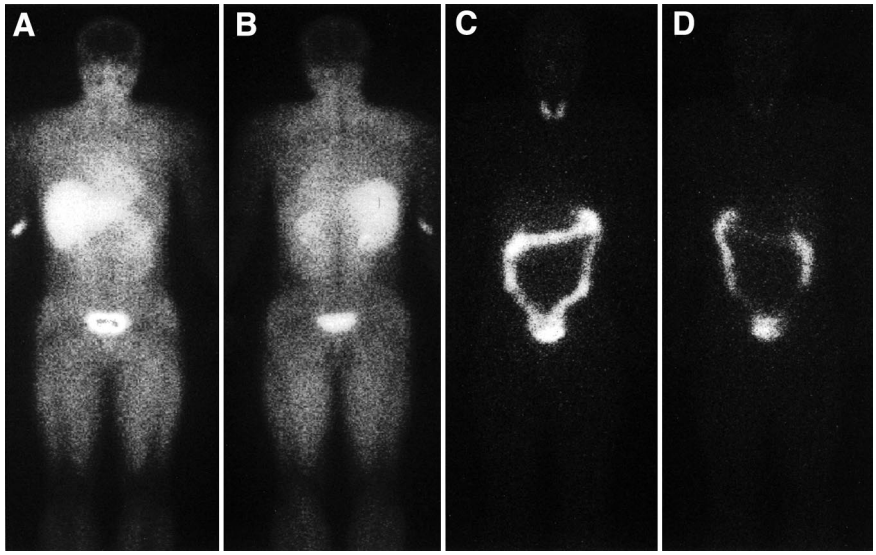

FIGURE 1. Typical immediate (0–30 min) anterior (A) and posterior (B) view, and 22-h anterior (C) and posterior (D) view images after ^{123}I-IAZA intravenous administration to volunteer. Images were obtained from volunteer 3 (27-y-old man) after injection of 207.2 MBq (5.62 mCi) ^{123}I-IAZA into right arm.

ysis, was negligible and therefore not expected to alter the distribution kinetics of the radiopharmaceutical. The injection site was also visible, to a lesser extent, on the immediate images of volunteer 5 (not shown).

There was a striking absence of radioactivity in the brains of all the volunteers in early- and intermediate-time images, indicating effective exclusion of ^{123}I-IAZA by the blood–brain barrier. Later images, however, showed some redistribution of radioactivity into the brain. Immediate, 1- to 2-h, and 3- to 4-h images also did not show thyroid or large intestine uptake; in fact, these organs did not become readily visible until the 20- to 24-h image acquisition time (Fig. 1).

During the determination of gastrointestinal tract counts, only the large intestine and gallbladder counts were included because the small intestine was never clearly distinguishable in any of the images. Because the radioactivity entering the intestinal tract from the gallbladder constituted a small fraction of the dose (<10% of biologically eliminated activity), it was only visible when either concentrated in a small area (i.e., the gallbladder) or 20 h after dose administration, after a substantial portion of the dose was eliminated from the rest of the body. Some concentration of intestinal activity was evident in the 6- to 8-h image, but at that time it was either localized in the junction of the ileum and the ascending colon or already in the initial part of the ascending colon. In each case, this activity was included as part of the large intestine ROI.

A summary of radiation dose estimates for all volunteers for the 2-h bladder void time is shown in Table 1. The source organs were liver, kidneys, thyroid, and RB, and the activities in these organs were assumed to be uniformly distributed. Radiation dose caused by activity observed in the urinary bladder and the gastrointestinal tract was calculated separately. Although the reference adult phantom used for dose estimates in men does predict radiation dose to the ovaries as well as testis, the adult female phantom does not predict the dose to the testis. Volunteers 4 and 6 were women.

TABLE 1
Radiation Dose Estimates for 4 Male and 2 Female Patients

Organ	Total dose	
	mGy/MBq	rad/mCi
Adrenals	8.5E-03 ± 8.3E-04	3.2E-02 ± 3.1E-03
Brain	5.5E-03 ± 5.3E-04	2.0E-02 ± 2.0E-03
Breasts	4.7E-03 ± 4.7E-04	1.7E-02 ± 1.7E-03
GB wall	1.2E-02 ± 1.7E-03	4.6E-02 ± 6.1E-03
LLI wall	5.6E-02 ± 1.2E-02	1.7E-01 ± 7.9E-02
Small intestine	2.4E-02 ± 5.1E-03	7.2E-02 ± 3.3E-02
Stomach	8.7E-03 ± 9.5E-04	3.2E-02 ± 3.5E-03
ULI wall	5.0E-02 ± 1.2E-02	1.5E-01 ± 7.0E-02
Heart wall	7.2E-03 ± 7.4E-04	2.7E-02 ± 2.7E-03
Kidneys	1.9E-02 ± 9.2E-04	7.0E-02 ± 3.5E-03
Liver	1.4E-02 ± 3.0E-03	5.2E-02 ± 1.1E-02
Lung	6.7E-03 ± 7.3E-04	2.5E-02 ± 2.7E-03
Muscle	7.1E-03 ± 5.8E-04	2.6E-02 ± 2.2E-03
Ovaries	1.8E-02 ± 3.1E-03	6.7E-02 ± 1.1E-02
Pancreas	9.0E-03 ± 8.7E-04	3.3E-02 ± 3.3E-03
Red marrow	7.2E-03 ± 6.3E-04	2.7E-02 ± 2.4E-03
Bone surfaces	1.2E-02 ± 1.1E-03	4.5E-02 ± 3.9E-03
Skin	4.5E-03 ± 3.8E-04	1.7E-02 ± 1.4E-03
Spleen	7.7E-03 ± 6.6E-04	2.8E-02 ± 2.5E-03
Testes	7.0E-03 ± 1.9E-04	2.6E-02 ± 6.9E-04
Thymus	6.2E-03 ± 6.2E-04	2.3E-02 ± 2.3E-03
Thyroid	4.4E-02 ± 1.4E-02	1.4E-01 ± 7.9E-02
UB wall	6.3E-02 ± 8.7E-03	2.0E-01 ± 8.9E-02
Uterus	1.6E-02 ± 1.4E-03	5.8E-02 ± 5.5E-03
TB	8.0E-03 ± 7.1E-04	3.0E-02 ± 2.6E-03
Effective dose equivalent	2.1E-02 ± 2.8E-03*	7.9E-02 ± 1.0E-02†
Effective dose	2.2E-02 ± 2.4E-03*	8.0E-02 ± 9.1E-03†

*mSv/MBq.
†rem/mCi.
GB = gallbladder; LLI = lower large intestinal; ULI = upper large intestinal; UB = urinary bladder.
Values are mean ± SD for ^{123}I-IAZA using 2-h bladder void time.

The organs receiving the greatest radiation dose were the thyroid, upper and lower large intestinal wall, urinary bladder wall, and small intestine. The bladder was an important source organ, because >90% of the physiologically eliminated radioactivity was excreted by the kidneys. Encouraging the patients to urinate frequently, especially during the first 8 h after dose administration, would substantially reduce the radiation dose to the urinary bladder wall.

DISCUSSION

The primary source organ for the majority of target organs listed in Table 1 was the RB. Exceptions were the lower large intestinal wall, upper large intestinal wall, small intestine, kidneys, liver, thyroid, and urinary bladder wall, all of which were their own primary sources and targets. For the urinary bladder and upper large intestinal and lower large intestinal walls, it was assumed that the source of activity was the organ content and not the organ wall. The primary contributors for the uterus and TB varied with the bladder void time, with the RB and the urinary bladder acting as the primary contributors for a 2-h void time. Similarly, for the effective dose (*16*), the primary source organ was the colon or the urinary bladder.

The main sources of error involved in the dose estimates presented in Table 1 include the lack of attenuation correction and removal of overlying background from the ROI source organ activity determinations. The failure to remove overlying background activity from the organ ROI will overestimate the radiation dose; however, this will be partially compensated for by the lack of attenuation correction, which will result in underestimating the dose. The assumption of uniform distribution of radioactivity in an organ is another important factor when using the MIRD schema. This is especially important for organs such as the large intestine, where gastrointestinal tract transit time determines radioactivity localization at the time of image acquisition, and for the kidneys, where the highest activity concentration after ^{123}I-IAZA administration was visible in the renal pelvis area. Not only will different parts of these organs receive variable radiation doses, but also any overlap ROI calculation involving these organs will introduce errors in the ROI counts determination of all the overlapping organs. A final important source of error was the accuracy of ROI drawing, which was estimated at ±10% based on 5 repeated drawings of the same ROI.

The radioactivity in the thyroid gland was thought to be caused by metabolic deiodination of ^{123}I-IAZA, with subsequent active accumulation of ^{123}I-iodide. For the purpose of this study, the radioactivity in the thyroid gland was considered irreversibly bound and was eliminated with the 13.2-h decay half-life of the isotope. The volunteers in this study received a single oral dose of Lugol's solution at the time of ^{123}I-IAZA injection. Because iodine incorporation into the thyroid gland takes place with a 6- to 8-h half-life, it may be possible to further decrease the radiation dose to the thyroid by administering Lugol's solution earlier in the protocol (*17,18*). Although a single dose did not completely block the thyroid, in volunteer 6 the thyroid gland was virtually undetectable even at the time of the 20- to 24-h image acquisition.

Table 2 compares ^{123}I-IAZA and several radiopharmaceuticals that are either commercially available or are being investigated as potential clinically useful imaging agents. Dose estimates are for adults with a 2-h bladder void time. These data emphasize the low doses from ^{123}I-IAZA, because the ^{123}I-IAZA radiation dosimetry is comparable with some ^{99m}Tc-labeled agents. ^{99m}Tc-sestamibi, for example, is commonly given as a 1.1-GBq injection, resulting in a TB dose of 5 mGy, whereas ^{123}I-IAZA, clinically given as a 370-MBq dose, will produce a TB dose of approximately 3 mGy.

The TB RT calculated using gamma camera ROI information and the pharmacokinetic MRT, which was calculated as the area under the concentration–time moment curve divided by the area under the concentration–time curve, are not identical in concept. Individual organ RTs represent the distribution of activity in various organs in the body as identified by ROI analysis, and the RB represents the tissues and organs with similar distribution characteristics; the whole-body RT of the tracer is the sum of the RTs of each of these components. In multicompartmental phar-

TABLE 2
Dosimetry Estimates Comparison Between ^{123}I-IAZA and Several Other Radiopharmaceuticals for Adults Using 2-Hour Bladder Void Time

Generic name	ULI	LLI	Thyroid	Urinary bladder wall	Total body	Reference
^{123}I-IAZA	5.0E-02	5.6E-02	4.4E-02	6.3E-02	8.0E-03	This study
^{123}I-Tropane	4.3E-02	4.6E-02	5.7E-02	9.7E-02	N/A EDE = 3.2E-02	*17*
^{131}I-Iodobenguane sulfate	N/A	N/A	9.2E-02	8.0E-01	6.2E-02	*19*
^{99m}Tc-Bicisate	1.6E-02	1.3E-02	3.5E-03	3.0E-02	2.4E-03	*20*
^{99m}Tc-Sestamibi	4.9E-02	3.5E-02	6.2E-03	1.8E-02	4.6E-03	*21*

ULI = upper large intestinal wall; LLI = lower large intestinal wall; N/A = not provided in product monograph; EDE = effective dose equivalent (mSv/MBq).

Values are in mGy/MBq.

macokinetic analysis of serum radioactivity, the organs representing the RB would all constitute a single compartment, whereas organs with different MRTs would each constitute a separate compartment. To compare these approaches, it is important to use pharmacokinetic data representing total radioactivity rather than the radiopharmaceutical alone because no differentiation is possible with gamma camera analysis. After the serum-based pharmacokinetic analysis of total radioactivity after ^{123}I-IAZA administration in these volunteers, only 2 compartments were discernible, as can be seen from the plot of total radioactivity in Figure 2 (*12*). However, gamma camera scintigraphic images of the WB appear to show at least 4 regions with elevated uptake: the liver, kidney, thyroid, and RB. An attempt was made to discern whether these regions were separate compartments of a multicompartmental pharmacokinetic model.

An explanation for this apparent discrepancy between the serum-based and scintigraphic-based models can be obtained through inspection of the different sources of data sampled by each technique. We observed that the scintigraphic-based RTs calculated for the liver and kidney were 7.35 ± 1.05 h and 7.53 ± 1.47 h, respectively. A 1-way ANOVA (power of significance = 0.05) did not detect statistically significant differences in the organ RTs and, hence, both the liver and the kidney could be ascribed to the same pharmacokinetic compartment (Table 3). Because the thyroid represents <0.5% of the AB cumulated activity, it would not be discernable as a separate compartment by serum analysis. TB imaging data represent activity mainly caused by blood and are therefore expected to be quantitatively similar to the serum-based model.

Classic pharmacokinetic sample acquisition methods generally rely on venous blood samples. Consequently, only quantitatively important compartments with different MRTs can be identified. In the case of ^{123}I-IAZA, the very small fraction of dose accumulated in the thyroid would not be detected by serum analysis, despite the long MRT of activity in this organ. Furthermore, serum analysis would group all organs with similar MRTs into a single compartment, regardless of their respective concentrations of radioactivity. This is in keeping with the tenet that if the rate of change of activity of different organs (as represented by ROIs) is similar, then they can be attributed to the same compartment (*22*).

TABLE 3
Mean Residence Time Estimates for Various Organs for 6 Healthy Volunteers

Organ	Volunteer no. 1	2	3	4	5	6	Mean	SD
Liver	8.00	6.82	6.85	7.12	9.13	6.19	7.35	1.05
Kidney	7.86	5.45	7.39	6.32	8.84	9.29	7.53	1.47
Thyroid	8.29	6.60	7.11	6.31	7.55	5.25*	7.17	0.79
RB	7.02	6.21	6.09	6.60	7.41	6.12	6.57	0.54

*Thyroid ROI absent.
Data are in hours and are based on WB scintigraphic image analysis at 5 time points within 24-h period after ^{123}I-IAZA administration.

The distribution phase of total radioactivity, as determined from the pharmacokinetic analysis of blood samples, was found to represent only 5% of the overall AUC (*12*). With a 30-min image acquisition time, this distribution phase was too short to be discernable with gamma camera scintigraphic techniques. It was not possible to decrease the whole-body acquisition time caused by gamma camera sensitivity and the amount of ^{123}I-IAZA injected. Thus, the source organs were the sources of radioactivity not by virtue of longer RTs, but because they had relatively higher affinity for the radioactive components, which resulted in greater volumes of distribution of total radioactivity.

In addition to the estimate of the TB RT and MRT, the 2 methods also can be used independently to determine the biologic elimination routes of total radioactivity from the body. In pharmacokinetic analysis, the fraction eliminated in urine was determined directly by analyzing the pooled 0- to 28-h urine samples. The remainder of the dose was assumed to be excreted through the gut (*12*). Scintigraphic analysis proceeds in the opposite order: The fraction of radioactivity entering the gut is determined from the images, and then remaining loss of activity is considered to be eliminated in the urine.

Gamma camera ROI analysis was used to predict the percentage of total radioactivity excreted in urine for volunteer 3, who had failed to collect a final urine sample. A renal clearance of 111 mL/min was determined for this individual, which was comparable with those of the other 5 volunteers and showed an advantage of gamma camera scintigraphic analysis to compensate for the subject's noncompliance.

Table 4 shows estimates of TB RT and MRT and the percentage dose eliminated in urine using the 2 methods for

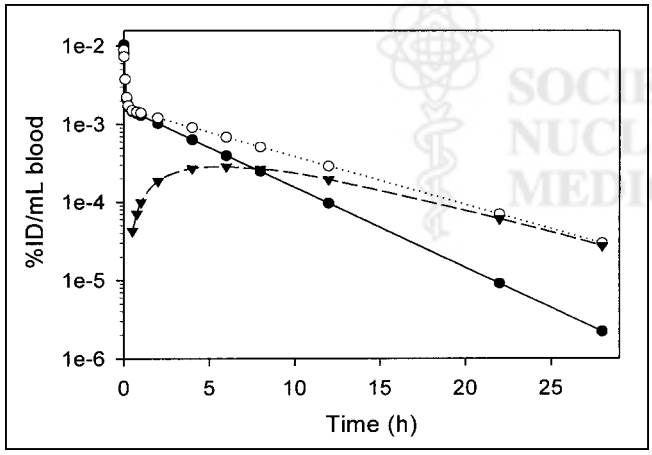

FIGURE 2. Plots of mean dose-normalized disposition of total radioactivity and ^{123}I-IAZA (experimental data) and radioactive metabolites (derived data) in human volunteers after ^{123}I-IAZA administration. Data are plotted as percentage injected dose per milliliter of blood and are not decay corrected. ○ = total radioactivity; ● = ^{123}I-IAZA; ▼ = radioactive metabolites. (Reprinted with permission of (*12*).)

TABLE 4
Comparison of Gamma Camera and Serum-Based Pharmacokinetic Methods Used to Estimate MRT and RT and Percentage of Total Radioactivity Eliminated in Urine

	Gamma camera		Pharmacokinetic*		PK/gamma camera	
Volunteer no.	RT_{TB} (h)	Urine (%)	MRT_{TB} (h)	Urine (%)	RT_{TB}/MRT_{TB}	Urine
1	7.44	88.9	7.25	95.3	0.97	1.07
2	7.01	92.0	7.28	85.1	1.04	0.92
3	6.88	92.8	5.95	64.4†	0.86	0.069
4	6.85	87.5	6.52	93.5	0.95	1.07
5	7.38	88.7	7.67	91.2	1.04	1.03
6	7.60	88.0	6.40	97.0	0.84	1.10

*Reproduced with permission of (*12*).
†Incomplete urine collection (sample missed at end of collection interval).
PK = pharmacokinetic method.

each of the volunteers in this study. Percentage dose in urine was based on biologic elimination routes only and did not include clearance caused by physical decay of the radionuclide. Although the 2 methods used completely different approaches, included different arrays of assumptions, and had different errors associated with them, the resulting values were strikingly similar. This is expected when considering that the main sources of error for the ROI dataset would primarily affect the number of counts in a given ROI. Serial images on the same patient would include similar ROI error terms but produce time–count-rate curves that were parallel to, but vertically displaced from, the true distribution.

Although pharmacokinetic analysis was expected to be more accurate than the gamma camera analysis, both methods produced similar estimates of the TB MRT and the renal elimination fraction for total radioactivity. Gamma camera ROI estimation of these parameters required correct identification of the TB ROI, which, according to Equation 1, directly relies on the activity estimates in 3 other ROIs: the WB, the gut, and the urinary bladder. However, gut activity determination depends on numerous other ROIs, including large intestine overlap regions with other organs and the organs that overlap with the large intestine (i.e., the liver and the kidneys). Consequently, the excellent correlation between pharmacokinetic and gamma camera estimates in these volunteers also confirmed the methodology of the ROI drawing and overlap resolution procedures described in the experimental section.

CONCLUSION

The dosimetric analysis of ^{123}I-IAZA in 6 healthy volunteers indicated that both disposition kinetics and favorable dosimetry support its clinical use for imaging tissue hypoxia. ^{123}I-IAZA has been shown to have comparable dosimetry with several currently marketed diagnostic radiopharmaceuticals. The excellent correlation between gamma camera–based and serum-based kinetic analyses suggested that detailed pharmacokinetic analysis during dosimetry studies can serve as an important aid in validating some of the assumptions made in estimation of location and transit times of radioactive molecules from scintigraphic images.

ACKNOWLEDGMENTS

IAZA was synthesized by Dr. Elena Atrazheva and radiolabeled by Ronald Schmidt. This research was supported in part through Alberta Cancer Board grant RI-14 and predoctoral scholarships from the Medical Research Council of Canada and the Alberta Heritage Foundation for Medical Research.

REFERENCES

1. Mannan RH, Somayaji VV, Lee J, et al. Radioiodinated 1-(5-iodo-5-deoxy-β-D-arabinofuranosyl)-2-nitroimidazole (iodoazomycin arabinoside: IAZA), a novel marker of tissue hypoxia. *J Nucl Med.* 1991;32:1764–1770.
2. Mercer JR, Mannan RH, Somayaji VV, et al. Sugar-coupled 2-nitroimidazoles: novel in vivo markers of hypoxic tumor tissue. In: Maddalena DJ, Snowdon GM, Boniface GR, eds. *Advances in Radiopharmacology, Proceedings of the 6th International Symposium on Radiopharmacology*. Wollongong, Australia: Wollongong University Printery Services; 1990:104–113.
3. Parliament MB, Chapman JD, Urtasun RC, et al. Non-invasive assessment of human tumour hypoxia with ^{123}I-iodoazomycin arabinoside: preliminary report of a clinical study. *Br J Cancer.* 1992;65:90–95.
4. Urtasun RC, Parliament MB, McEwan AJ, et al. Measurement of hypoxia in human tumours by non-invasive SPECT imaging of iodoazomycin arabinoside. *Br J Cancer.* 1996;74(suppl):S209–S212.
5. Groshar D, McEwan AJB, Parliament MB, et al. Imaging tumor hypoxia and tumor perfusion. *J Nucl Med.* 1993;34:885–888.
6. Al-Arafaj A, Ryan EA, Hutchison K, et al. An evaluation of iodine-123 iodoazomycin arabinoside as a marker of localized tissue hypoxia in patients with diabetes mellitus. *Eur J Nucl Med.* 1994;21:1338–1342.
7. Lythgoe MF, Williams SR, Wiebe LI, et al. Autoradiographic imaging of cerebral ischaemia using a combination of blood flow and hypoxic markers in an animal model. *Eur J Nucl Med.* 1997;24:16–20.
8. Lythgoe MF, Williams SR, Busza AL, et al. The relationship between magnetic resonance diffusion imaging and autoradiographic markers of cerebral blood flow and hypoxia in an animal stroke model. *Magn Reson Med.* 1999;41:706–714.
9. McEwan AJB, Skeith KJ, Mannan RH, et al. Iodine-123 iodoazomycin arabinoside (IAZA) may have a role in imaging rheumatoid arthritis [abstract]. *J Nucl Med.* 1997;38(suppl):300P–301P.
10. Vinjamuri S, O'Driscol K, Maltby P, et al. Identification of hypoxic regions in traumatic brain injury. *Clin Nucl Med.* 1999;24:891–892.
11. Snyder W, Ford M, Warner G, Watson S. "S" absorbed dose per unit cumulated activity for selected radionuclides and organs. *MIRD Pamphlet No. 11*. New York, NY: Society of Nuclear Medicine; 1975.
12. Stypinski D, Wiebe LI, McEwan AJ, et al. Clinical pharmacokinetics of ^{123}I-IAZA in healthy volunteers. *Nucl Med Commun.* 1999;20:559–567.
13. Mannan RH. *Novel Non-Invasive Markers of Tumor Hypoxia* [dissertation]. Edmonton, Alberta, Canada: University of Alberta; 1991.
14. Loevinger R, Budinger TF, Watson EE. *MIRD Primer for Absorbed Dose Calculations.* New York, NY: Society of Nuclear Medicine; 1988.
15. Ediss C, Tam YK. An interactive computer program for determining areas bounded by drug concentration curves using Lagrange interpolation. *J Pharmacol Toxicol Methods.* 1995;34:164–168.
16. Stabin MG. MIRDOSE: personal computer software for internal dose assessment in nuclear medicine. *J Nucl Med.* 1996;37:538–546.
17. Mozley PD, Stubbs JB, Kim HJ, et al. Dosimetry of an iodine-123-labeled tropane to image dopamine transporters. *J Nucl Med.* 1996;37:151–159.
18. Nunan TO, Coakley AJ, Elliott AT. Notes for guidance on clinical administration of radiopharmaceuticals and use of sealed radioactive sources, thyroid blocking. *Nucl Med Commun.* 2000;21(suppl):S29–S30.
19. ^{131}I-MIBG [product monograph]. Montreal, Quebec, Canada: Draximage; 1997.
20. Neurolite [product monograph]. Toronto, Ontario, Canada: Nycomed Amersham; 1997.
21. Cardiolite [product monograph]. Montreal, Quebec, Canada: DuPont; 1997.
22. Gibaldi M, Perrier D. *Pharmacokinetics.* New York, NY: Marcel Dekker, Inc; 1982:45–111.